



OPEN ACCESS

EDITED BY

Faisal Ur Rahman Awan,
Edith Cowan University, Australia

REVIEWED BY

Hongjian Zhu,
Yanshan University, China
Nidhal Badrouchi,
University of North Dakota, United States

*CORRESPONDENCE

Sijie He,
✉ hesijie@cqust.edu.cn

RECEIVED 06 January 2025

ACCEPTED 21 March 2025

PUBLISHED 28 March 2025

CITATION

Wang Y, Bao Z, Li Z, He S and Fang F (2025)
High-temperature and high-pressure online
nuclear magnetic resonance testing for CO₂
flooding in Daqingzijing Oilfield.
Front. Earth Sci. 13:1556179.
doi: 10.3389/feart.2025.1556179

COPYRIGHT

© 2025 Wang, Bao, Li, He and Fang. This is an open-access article distributed under the terms of the [Creative Commons Attribution License \(CC BY\)](https://creativecommons.org/licenses/by/4.0/). The use, distribution or reproduction in other forums is permitted, provided the original author(s) and the copyright owner(s) are credited and that the original publication in this journal is cited, in accordance with accepted academic practice. No use, distribution or reproduction is permitted which does not comply with these terms.

High-temperature and high-pressure online nuclear magnetic resonance testing for CO₂ flooding in Daqingzijing Oilfield

YuNing Wang^{1,2}, Zhidong Bao¹, Zhongcheng Li^{1,3,4}, Sijie He^{5*} and Feifei Fang⁵

¹College of Geosciences, China University of Petroleum (Beijing), Beijing, China, ²Research Institute of Petroleum Exploration and Development, PetroChina, Beijing, China, ³Research Institute of Exploration and Development, PetroChina Jilin Oilfield Company, Songyuan, China, ⁴State Key Laboratory of Petroleum Resource and Prospecting, China University of Petroleum (Beijing), Beijing, China, ⁵School of Petroleum Engineering, Chongqing University of Science and Technology, Chongqing, China

As global energy demand continues to grow, enhancing the recovery rate of mature oilfields has become an important research task. CO₂ flooding, as an effective enhanced oil recovery (EOR) technique, has received extensive attention in recent years. However, the multiphase flow and oil mobilization mechanisms during CO₂ flooding are not fully understood, particularly under the actual high-temperature and high-pressure conditions in oilfields. Optimizing CO₂ flooding techniques to improve recovery rates in these conditions has become an urgent issue. In this paper, high-temperature and high-pressure online nuclear magnetic resonance (NMR) testing technology is employed to simulate the formation conditions of the Daqingzijing Oilfield. Online NMR testing experiments are conducted with varying injection rates and flooding methods. The results indicate that regardless of slug size or injection rate, the remaining oil volume in both core samples is significantly reduced. Smaller slug sizes and lower injection rates result in less remaining oil and better displacement effect. As the slug size increases from 0.1 PV to 0.4 PV, the average recovery rate decreases by approximately 7%. Similarly, when the injection rate increases from 0.01 mL/min to 0.04 mL/min, the average recovery rate decreases by around 8%. Furthermore, there are significant differences in oil displacement effect among different flooding methods. The foam system exhibits the highest oil displacement effect, followed by water-gas alternating flooding, continuous gas injection, and finally water flooding followed by continuous gas injection. Compared to water flooding followed by continuous gas injection, continuous gas injection increases the average recovery rate by about 8%, water-gas alternating flooding increases it by about 13%, and the foam system increases it by about 18%. This study not only deepens the understanding of the CO₂ flooding process but also provides scientific basis and technical support

for formulating more reasonable CO₂ flooding schemes and improving recovery rates.

KEYWORDS

Daqingzijing Oilfield, CO₂ flooding, high-temperature and high-pressure, online nuclear magnetic resonance (NMR), recovery rate

1 Introduction

In recent years, with the continuous growth of global energy demand and the increasing awareness of environmental protection, enhancing oil recovery and developing clean and efficient energy utilization methods have become important topics in the petroleum industry. CO₂ flooding, as an effective EOR technique, has attracted considerable attention due to its ability to utilize the dissolution, expansion, and viscosity reduction effects of CO₂, which significantly improve the mobility of crude oil (Liang et al., 2016; Tang et al., 2021; Tang et al., 2022). Especially in complex geological conditions such as those found in the Daqingzijing Oilfield (Dong, 2023; Gao, 2019; Liu et al., 2018), the application potential of CO₂ flooding is immense. However, the multiphase flow and oil mobilization mechanisms during the flooding process are not fully understood, which limits the further optimization and promotion of this technology.

Currently, research on CO₂ flooding has mostly focused on macroscopic displacement effects and numerical simulations (Kamali et al., 2015; Lu et al., 2024; Torabi et al., 2012; Dong et al., 2022; Ding et al., 2024; Xu et al., 2024; Lan et al., 2023; Guo et al., 2024; Hu et al., 2017). Kamali et al. (2015) conducted experiments on the joint optimization of CO₂-enhanced oil recovery and oil storage under immiscible, near-miscible, and miscible displacement conditions. The results showed that the recovery rates for miscible and near-miscible displacements were almost identical, while the recovery rate for immiscible displacement was approximately 18% lower. Dong et al. (2022) used microscopic visual oil displacement experiments and core flooding experiments to explore the oil displacement effects of different flooding methods and the “synergistic effect” mechanism between CO₂ and low interfacial tension viscoelastic fluids during their cooperative oil displacement process. Guo et al. (2024) took the H block of the Yanchang Oilfield as the research object and applied numerical simulation methods to optimize the development mode, gas injection timing, gas injection rate, bottomhole flowing pressure, and gas-water alternating cycle for two types of well groups in CO₂ flooding. The results indicated that the best gas injection effect occurred when the gas-water ratio was 1:1 and gas-water alternating injection was performed when the water content of the oil well was between 40% and 60%. Traditional testing methods often struggle to conduct real-time, dynamic monitoring under the actual high-temperature and high-pressure conditions of oilfields. Online NMR technology, as a non-destructive monitoring method, offers advantages such as real-time monitoring, dynamic response, and high resolution. It can monitor changes in fluid distribution and migration states within the core in real-time without interfering with the displacement process (Liu et al., 2017; Chen et al., 2024; Fu, 2023; Duan et al., 2021; Wang et al., 2017). Liu et al. (2017) conducted near-miscified CO₂ displacement experiments in

decane-saturated synthetic sand cores, using magnetic resonance imaging to study displacement front characteristics. The results show that under near-miscible conditions, vertical displacement is unstable above the minimum miscible pressure in the synthetic sand core. Duan et al. (2021) took methane gas as the experimental fluid to measure the variation of free and adsorbed methane production during shale gas exploitation, and combined with the physical simulation experiment of shale gas depletion development, studied the utilization characteristics and production variation rules of shale gas under different occurrence states. Through online NMR testing, the mobilization of crude oil after CO₂ injection, including displacement, aggregation, and distribution changes, can be observed intuitively, thus revealing the microscopic mechanisms of CO₂ flooding.

The primary objective of this study is to evaluate the effectiveness of high-temperature and high-pressure online NMR testing in monitoring CO₂ flooding processes in the Daqingzijing Oilfield. In this paper, the formation conditions of block Hei 125 and Block Hei 71 in Daqingzijing Oilfield were simulated, and the online nuclear magnetic displacement experiments were carried out with different CO₂ injection rates and displacement modes (water flooding followed by continuous gas flooding, water-gas alternating injection in a 1:1 ratio, continuous gas injection flooding, and foam system with gas alternating slug injection in a 1:1 ratio). The change of fluid distribution and recovery rate during CO₂ injection can be understood in real time by NMR. By comparing and analyzing the experimental results, the migration patterns of CO₂ within the core under different conditions were clarified, and its impact mechanism on crude oil mobilization was thoroughly discussed. This not only helps to deepen the understanding of the CO₂ flooding process but also provides a scientific basis for formulating more reasonable CO₂ flooding schemes and enhancing oil recovery rates.

2 Experimental procedures and methodology

2.1 Experimental scheme

The target blocks for this experiment are Blocks Hei 71 and Hei 125 in the Daqingzi-jing Oilfield, with a total of 15 groups, including seven groups from Block Hei 71 and eight groups from Block Hei 125. The experimental scheme is shown in Table 1.

The specific experimental scheme is as follows:

2.1.1 Water flooding followed by continuous gas flooding

After saturating the core sample with formation oil, one pore volume (PV) of heavy water is injected as the displacement medium.

TABLE 1 Experimental scheme for high-temperature and high-pressure online NMR testing of CO₂ flooding.

Block	Project	Quantity
Block Hei 71 (Rock Sample No. 23-1)	Water flooding followed by continuous gas flooding	1
	Water-gas alternating injection in a 1:1 ratio	3
	Continuous gas injection at different injection rates	3
Block Hei 125 (Rock Sample No. S21)	Water flooding followed by continuous gas flooding	1
	Water-gas alternating injection in a 1:1 ratio	3
	Continuous gas injection at different injection rates	3
	Foam system with gas alternating slug injection in a 1:1 ratio	1

TABLE 2 Basic data of rock samples.

Block	Core Number	Length/cm	Diameter/cm	Porosity/%	Permeability/ $\times 10^{-3} \mu\text{m}^2$
Hei 71	23-1	7.84	2.5	11.334	0.865
Hei 125	S21	4.65	2.5	10.291	3.101



FIGURE 1 Intelligent high-temperature and high-pressure magnetic resonance micro-nano flow experimental instrument.

Subsequently, the displacement medium is switched to CO₂, with an additional 1 PV injected at a constant rate of 0.01 mL/min. Throughout the process, the backpressure is maintained at 20 MPa. At key stages of the displacement process (based on injected volume), measurements are taken to capture the T₂ spectrum, layered T₂ distributions, and NMR imaging of the core to monitor fluid dynamics and saturation changes.

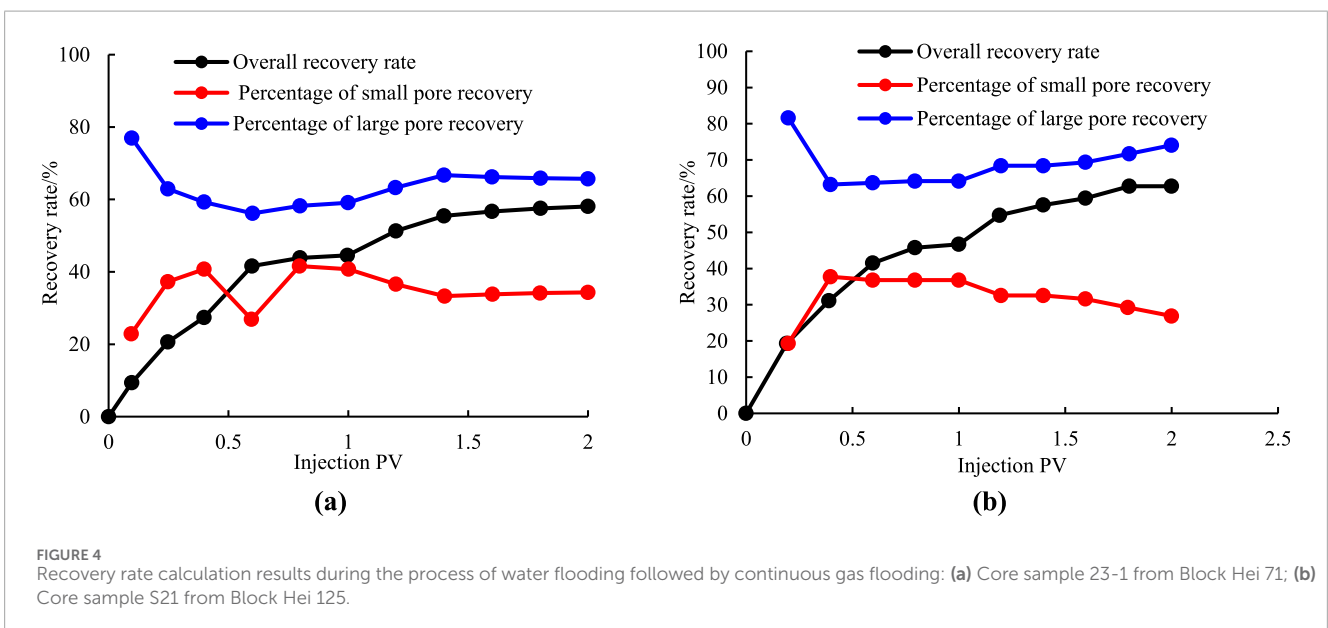
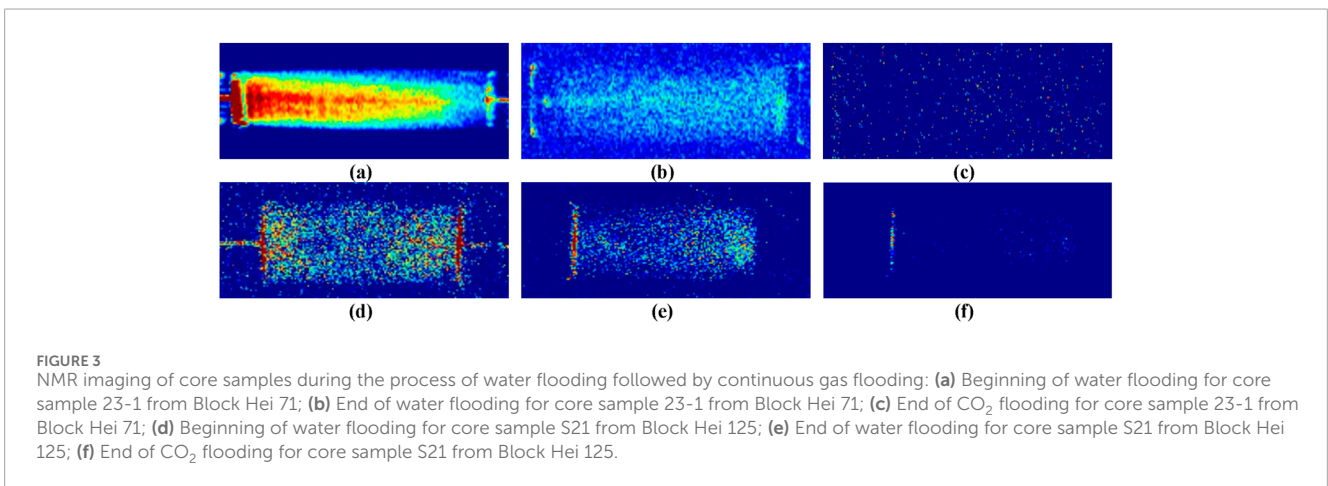
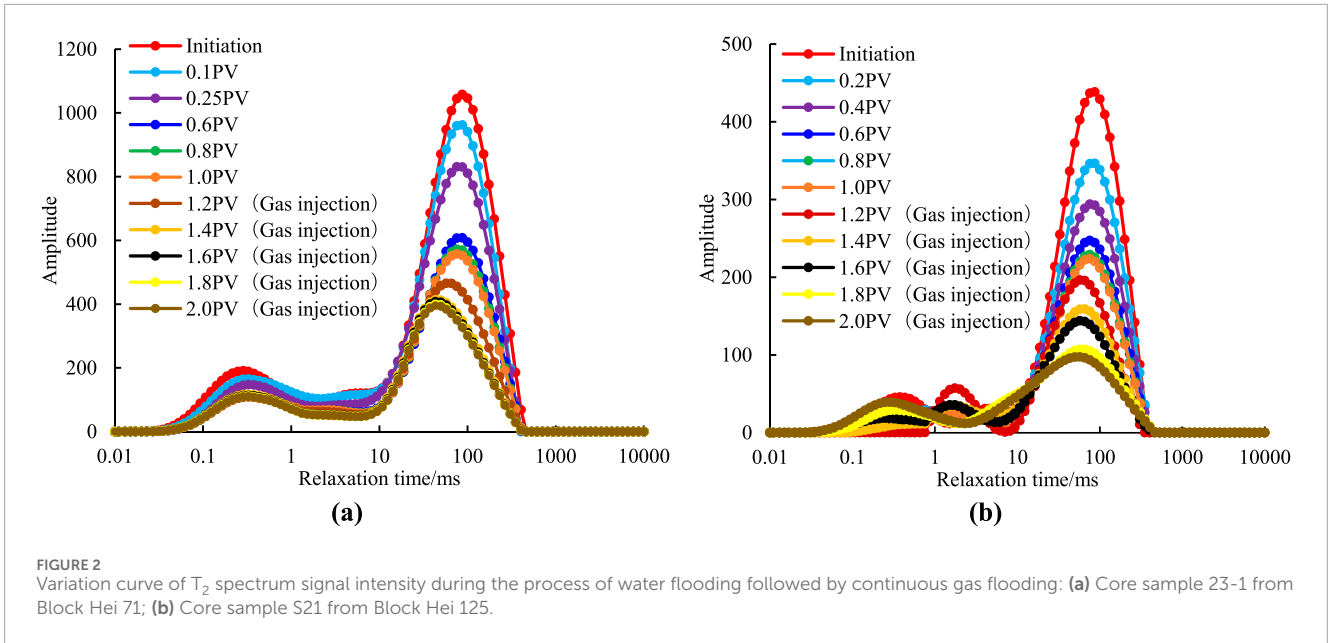
2.1.2 Water-gas alternating injection in a 1:1 ratio

This experiment employs alternating slugs of heavy water and CO₂ as displacement media. Online NMR displacement tests are conducted using two cores with varying slug sizes: 0.1 PV, 0.2 PV, and 0.4 PV. For the 0.1 PV and 0.2 PV slug groups, the total injected volume is set to 1.4 PV, while the 0.4 PV slug group requires a total injection of 1.6 PV. The injection rate is fixed at 0.01 mL/min, and the backpressure is stabilized at 20 MPa.

Real-time measurements of the T₂ spectrum, layered T₂ profiles, and NMR imaging are performed at multiple stages to analyze displacement efficiency and fluid distribution under alternating injection conditions.

2.1.3 Continuous gas injection at different injection rates

Using CO₂ as the sole displacement medium, this experiment investigates the impact of injection rates (0.01 mL/min, 0.02 mL/min, and 0.04 mL/min) on two core samples. Despite varying injection rates, the total injected volume is standardized at 1.4 PV for all groups. A constant backpressure of 20 MPa is applied, and NMR measurements (T₂ spectrum, layered T₂, and imaging) are systematically recorded at predefined intervals to evaluate how flow velocity influences fluid displacement patterns and pore-scale interactions.



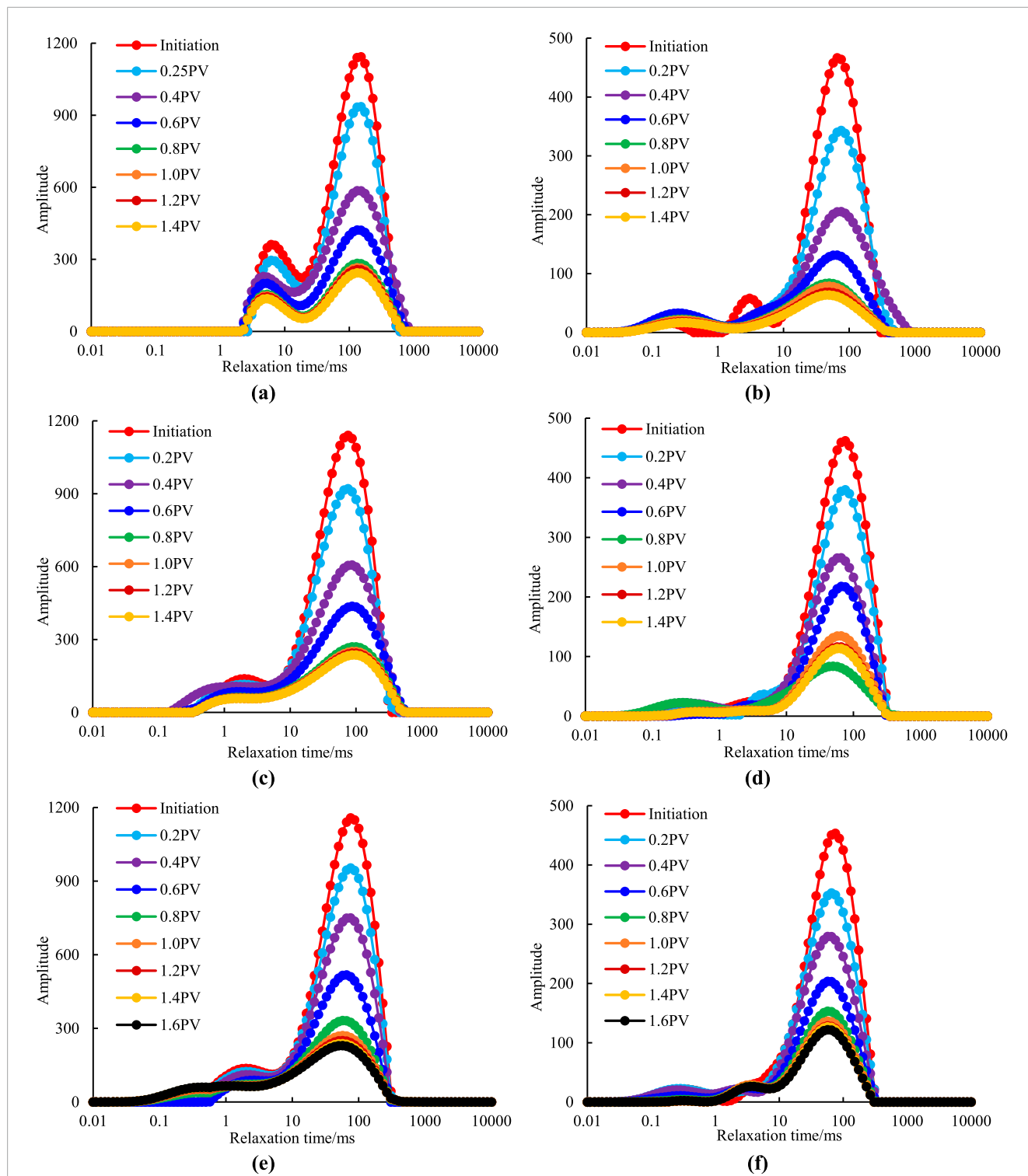


FIGURE 5
 Variation curves of T_2 spectrum signal intensity during the process of water-gas alternating injection in a 1:1 ratio: **(a)** Core sample 23-1 from Block Hei 71, slug size 0.1 PV; **(b)** Core sample S21 from Block Hei 125, slug size 0.1 PV; **(c)** Core sample 23-1 from Block Hei 71, slug size 0.2 PV; **(d)** Core sample S21 from Block Hei 125, slug size 0.2 PV; **(e)** Core sample 23-1 from Block Hei 71, slug size 0.4 PV; **(f)** Core sample S21 from Block Hei 125, slug size 0.4 PV.

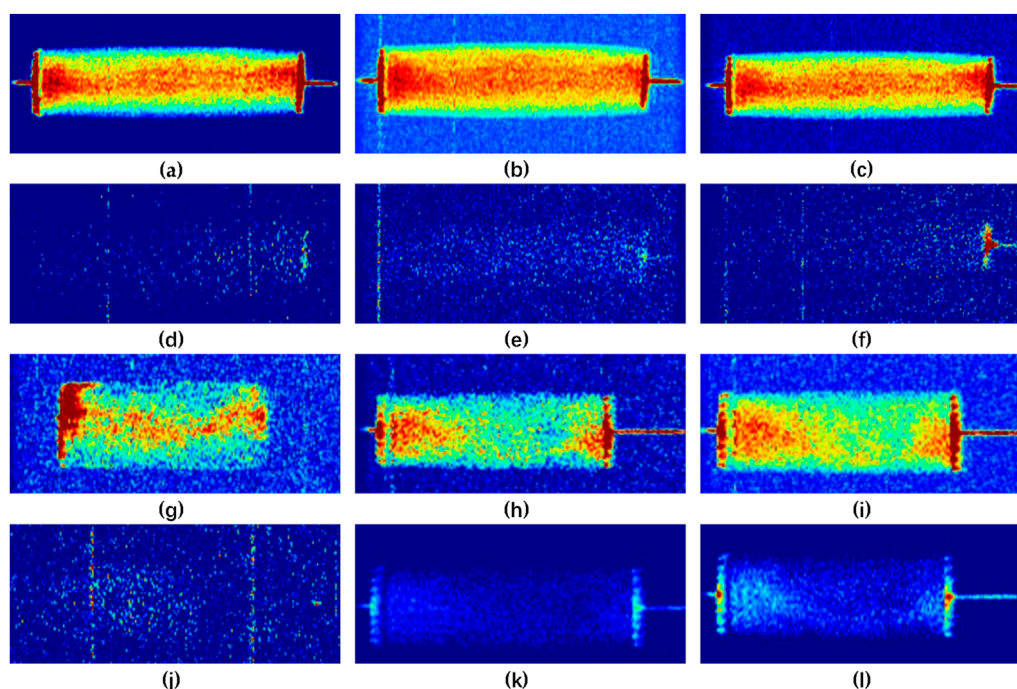


FIGURE 6

NMR imaging during the process of water-gas alternating injection in a 1:1 ratio: (a) Core sample 23-1 from Block Hei 71, slug size 0.1 PV, initial stage; (b) Core sample 23-1 from Block Hei 71, slug size 0.2 PV, initial stage; (c) Core sample 23-1 from Block Hei 71, slug size 0.4 PV, initial stage; (d) Core sample 23-1 from Block Hei 71, slug size 0.1 PV, end stage; (e) Core sample 23-1 from Block Hei 71, slug size 0.2 PV, end stage; (f) Core sample 23-1 from Block Hei 71, slug size 0.4 PV, end stage; (g) Core sample S21 from Block Hei 125, slug size 0.1 PV, initial stage; (h) Core sample S21 from Block Hei 125, slug size 0.2 PV, initial stage; (i) Core sample S21 from Block Hei 125, slug size 0.4 PV, initial stage; (j) Core sample S21 from Block Hei 125, slug size 0.1 PV, end stage; (k) Core sample S21 from Block Hei 125, slug size 0.2 PV, end stage; l. Core sample S21 from Block Hei 125, slug size 0.4 PV, end stage.

2.1.4 Foam system with gas alternating slug injection in a 1:1 ratio

Designed specifically for Rock Sample S21 from the Hei 125 Block, this protocol alternates between a foaming agent and CO₂ as displacement media. The total injection volume is 1.4 PV, delivered at a steady rate of 0.01 mL/min under a backpressure of 20 MPa. Special emphasis is placed on capturing the evolution of foam stability and mobility through T₂ spectral analysis, stratified T₂ relaxation data, and NMR imaging at critical stages. This setup aims to characterize the enhanced oil recovery mechanisms of foam systems under reservoir-like conditions.

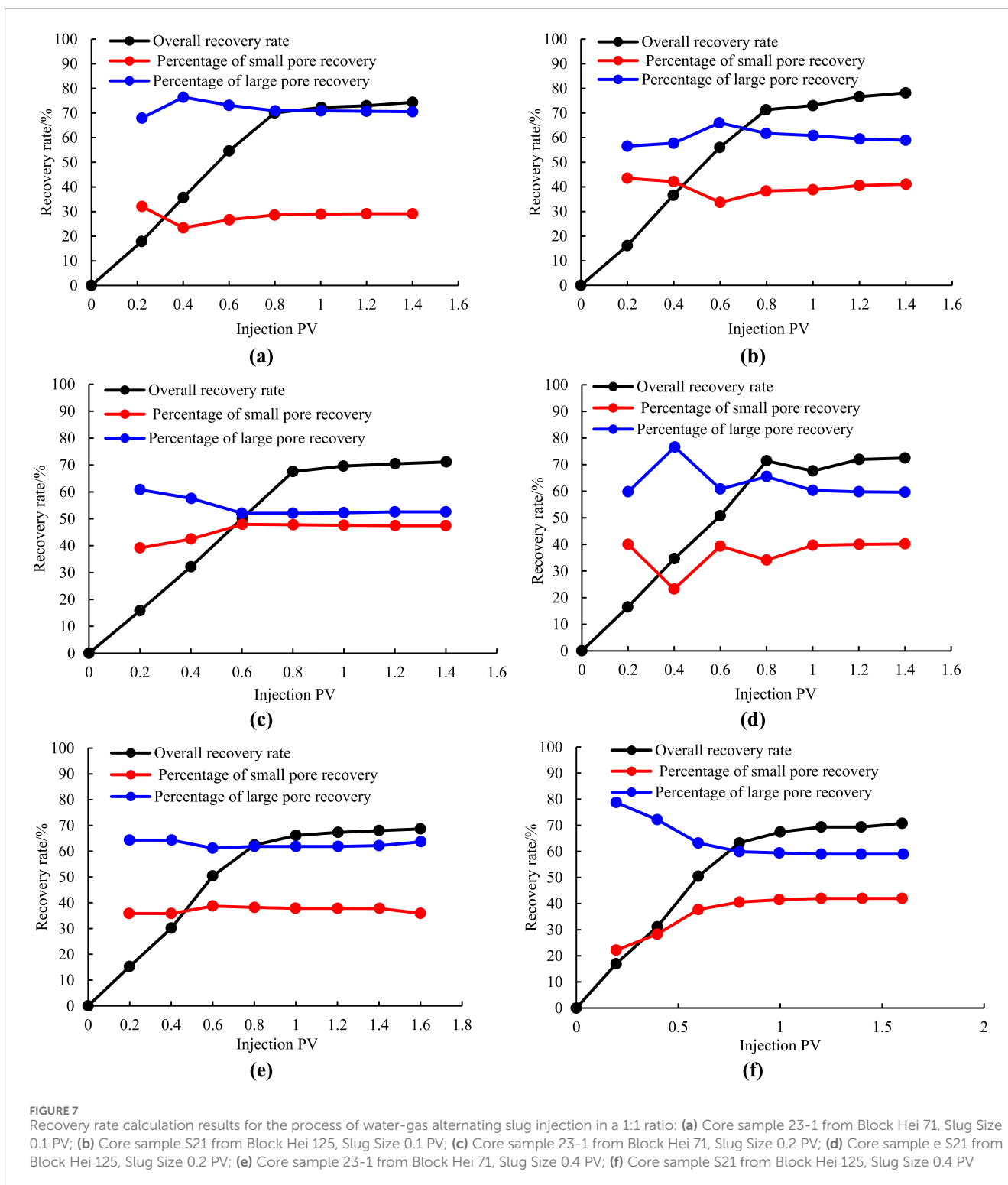
All procedures adhere to standardized monitoring protocols. Key parameters—including initial saturation, injection phase transitions, and final displacement endpoints—are rigorously tracked using synchronized NMR measurements. The backpressure system, injection pumps, and NMR acquisition timing are calibrated to ensure precision under high-pressure and high-temperature (HPHT) conditions. Data reproducibility is ensured by maintaining consistent environmental controls and measurement intervals across all experimental groups. In all experimental configurations, T₂ spectra, stratified T₂ relaxation profiles, and NMR imaging of the core samples were acquired at sequential displacement stages based on injected pore volumes. NMR T₂ relaxation time distributions were analyzed to infer pore size distributions and fluid saturation changes. Correlation analysis was performed to assess the relationship between NMR-derived

parameters and oil recovery efficiency and elucidate the mobilization mechanisms of CO₂ in targeting crude oil trapped across pores of distinct sizes.

2.2 Experimental materials and equipment

From each of the two blocks, one core sample was selected for experimentation. These two core samples underwent cutting, polishing, and porosity-permeability testing. The basic data of the rock samples are shown in Table 2.

To accurately simulate the formation conditions and ensure that the experimental results are close to actual field conditions, the oil used in this experiment was a simulated formation oil compounded in the laboratory. This simulated oil was prepared using degassed crude oil and natural gas produced from the wellbore, according to the original gas-oil ratio, original saturation pressure, and formation oil viscosity from the original high-pressure physical property data. In this experiment, there was a need to shield hydrogen ion signals in the water used as the displacement medium, so heavy water was employed. Additionally, this experiment also required the implementation of foam slug displacement, necessitating the preparation of a foam system that met the experimental requirements. The foam system used in this experiment was configured with sodium dodecyl sulfate as the foaming agent and polyacrylamide as the foam stabilizer. The



resulting foam system met the experimental requirements. The objective of this experiment was to provide a reference for the exploitation of the target blocks.

The equipment used in this experiment is the intelligent high-temperature and high-pressure magnetic resonance micro-nano flow experimental instrument (Model: MacroMR12-150H-

I), as shown in Figure 1. This equipment can achieve an overall experimental temperature of up to 160°C and an experimental pressure of up to 77.5 MPa. It is capable of conducting experiments such as online layered NMR of samples, T_1/T_2 spectrum analysis, oil-water distinction, and high-temperature and high-pressure displacement.

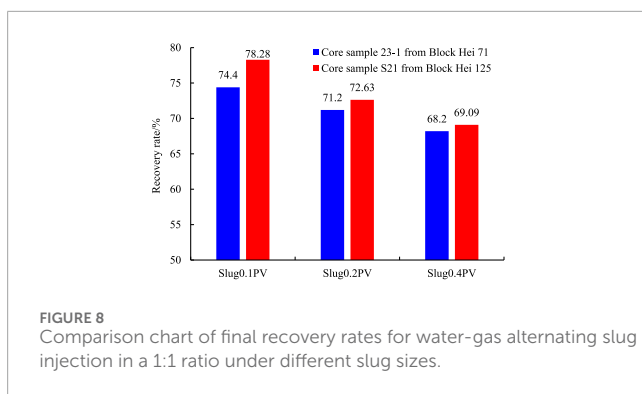


FIGURE 8
Comparison chart of final recovery rates for water-gas alternating slug injection in a 1:1 ratio under different slug sizes.

2.3 Experimental procedures

The specific steps for the high-temperature and high-pressure online NMR testing experiment with CO₂ flooding are as follows.

1. After cleaning and drying the core samples, measure their porosity and permeability.
2. Install the experimental cores into the NMR holder, apply a confining pressure of 25MPa, and displace 5 PV of heavy water. Then, begin the oil displacement process while monitoring the T₂ signal intensity in real-time until no further change is observed. This completes the simulation of the formation containing irreducible water.
3. Set the backpressure to 20 MPa and use a booster pump to pressurize the CO₂ to a supercritical state. Maintain a constant pressure difference of 5 MPa between the confining pressure and the displacement pressure using a confining pressure circulation pump. The subsequent specific steps for different experimental schemes are as follows:
 - (1) Water flooding followed by continuous gas flooding: Inject heavy water at a rate of 0.01 mL/min to initiate water flooding. After injecting 1 PV, switch to CO₂ injection at the same rate.
 - (2) Water-gas alternating injection in a 1:1 ratio: Begin with alternating water and gas slug displacement at a flow rate of 0.01 mL/min. After each water (or gas) slug injection, purge the pipeline of any remaining liquid (or gas) before proceeding to the next injection.
 - (3) Continuous gas injection at different injection rates: Initiate CO₂ displacement at injection rates of 0.01 mL/min, 0.02 mL/min, and 0.04 mL/min, respectively.
 - (4) Foam system with gas alternating slug injection in a 1:1 ratio: Begin with alternating CO₂ and foam slug displacement at a flow rate of 0.01 mL/min. After each foam (or gas) slug injection, purge the pipeline of any remaining foam or gas before proceeding to the next injection.
4. During the displacement process, conduct T₂, layered NMR, and NMR imaging measurements until the experiment is completed.

3 Results and discussion

3.1 Water flooding followed by continuous gas flooding

The results of the high-temperature and high-pressure online NMR testing for CO₂ flooding under the method of water flooding followed by continuous gas flooding for two core samples are shown in Figures 2, 3 below.

As can be seen from Figure 2, both core samples exhibit two peaks during the displacement process, with the highest T₂ signal intensity occurring at the initial state, reaching 1,050 and 450 respectively. As the displacement time increases, the T₂ signal intensity gradually decreases for both samples. The lowest T₂ signal intensity peaks occur at 2.0 PV (when switching to gas flooding), decreasing to 370 and 90 respectively.

Before the water flooding process begins, by observing the cores, we can gain a detailed understanding of the initial distribution characteristics of the remaining oil in the cores. Figure 3 shows that as water flooding progresses, the amount of remaining oil in both core samples decreases. When the water flooding process ends, the amount of remaining oil in both samples has dropped to a relatively low level. This change indicates that the water flooding effect is significant, with the water component effectively displacing the oil component through the advancement in the rock pores. When switching to continuous CO₂ flooding until the end, the amount of remaining oil in both core samples decreases again significantly.

As shown in Figure 4, the recovery rates at the end of water flooding for the two core samples are 44.55% and 46.58% respectively. During the water flooding stage, the recovery rate from large pores (relaxation time >50 ms) accounts for a high proportion. As water flooding progresses, the proportion of small pores gradually increases. After switching to gas injection, the overall recovery rates of the two core samples increase by about 14% and 16% respectively. During the gas injection process, the proportion of recovery rate from large pores increases, while the proportion of recovery rate from small pores decreases.

3.2 Water-gas alternating injection in a 1:1 ratio

The results of the high-temperature and high-pressure online NMR tests for CO₂ flooding under the method of water-gas alternating injection in a 1:1 ratio for the two core samples is shown in Figures 5, 6 below.

As can be observed from Figure 5, during the displacement process of water-gas alternating injection in a 1:1 ratio, the T₂ spectrum curve for Core Sample 23-1 from the Block Hei 71, under a slug size of 0.1 PV, exhibits two distinct peaks, whereas under other conditions, only one prominent peak is evident. Across all conditions, the highest peak of T₂ signal intensity occurs at the initial stage of displacement. For Core Sample 23-1 from the Block Hei 71, the peak T₂ signal intensities under three different slug sizes all

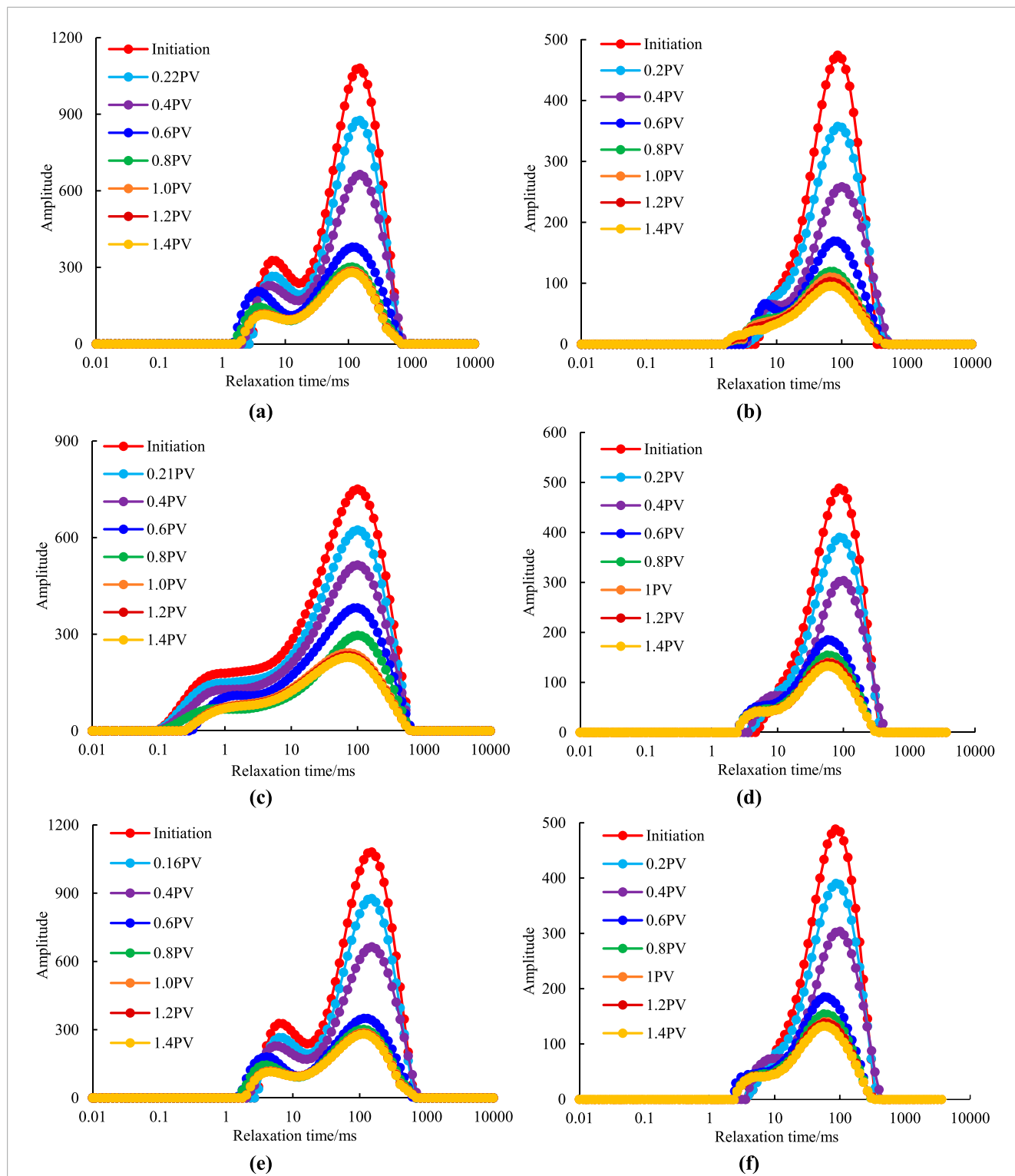


FIGURE 9 Variation curves of T_2 spectrum signal intensity during continuous gas injection at different injection rates: (a) Core sample 23-1 from Block Hei 71, injection rate 0.01 mL/min; (b) Core sample S21 from Block Hei 125, injection rate 0.01 mL/min; (c) Core sample 23-1 from Block Hei 71, injection rate 0.02 mL/min; (d) Core sample S21 from Block Hei 125, injection rate 0.02 mL/min; (e) Core sample 23-1 from Block Hei 71, injection rate 0.04 mL/min; (f) Core sample S21 from Block Hei 125, injection rate 0.04 mL/min.

approximate 1,200. Similarly, for Core Sample S21 from the Block Hei 125, the peak T_2 signal intensities under three different slug sizes all approximate 500. As the displacement time increases, the signal

intensity gradually decreases, with the lowest T_2 signal intensity peaks occurring at the end of the displacement process. For Core Sample 23-1 from the Block Hei 71, the lowest T_2 signal intensities

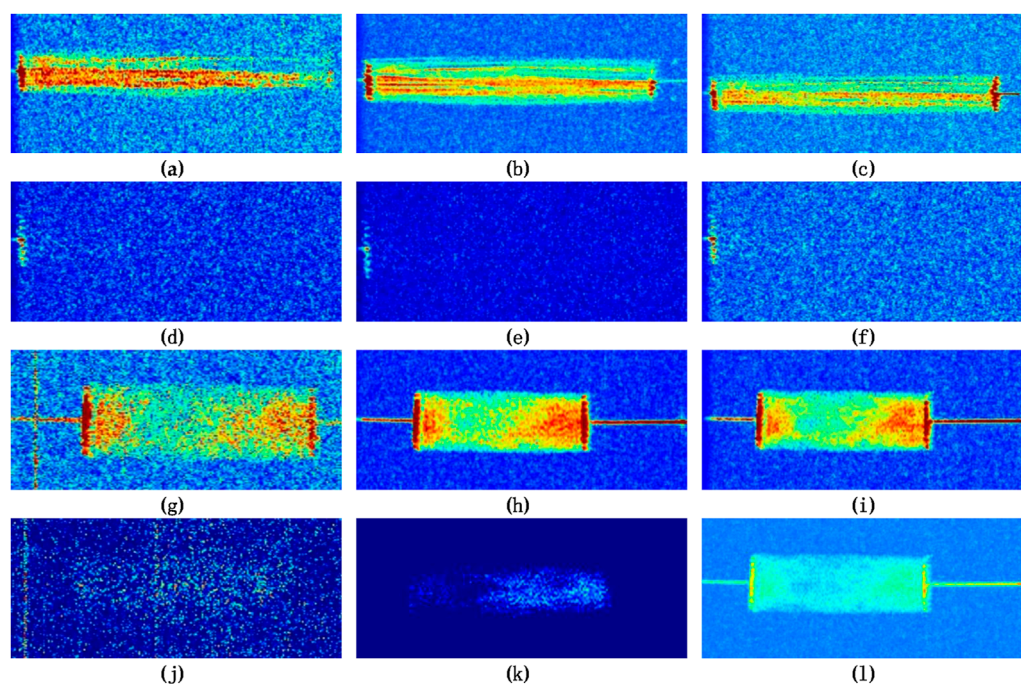


FIGURE 10

NMR imaging during continuous gas injection at different injection rates: (a) Core sample 23-1 from Block Hei 71, injection rate 0.01 mL/min, initial stage; (b) Core sample 23-1 from Block Hei 71, injection rate 0.02 mL/min, initial stage; (c) Core sample 23-1 from Block Hei 71, injection rate 0.04 mL/min, initial stage; (d) Core sample 23-1 from Block Hei 71, injection rate 0.01 mL/min, end stage; (e) Core sample 23-1 from Block Hei 71, injection rate 0.02 mL/min, end stage; (f) Core sample 23-1 from Block Hei 71, injection rate 0.04 mL/min, end stage; (g) Core sample S21 from Block Hei 125, injection rate 0.01 mL/min, initial stage; (h) Core sample S21 from Block Hei 125, injection rate 0.02 mL/min, initial stage; (i) Core sample S21 from Block Hei 125, injection rate 0.04 mL/min, initial stage; (j) Core sample S21 from Block Hei 125, injection rate 0.01 mL/min, end stage; (k) Core sample S21 from Block Hei 125, injection rate 0.02 mL/min, end stage; (l) Core sample S21 from Block Hei 125, injection rate 0.04 mL/min, end stage.

under three different slug sizes are 300, 280, and 120, respectively. For Core Sample S21 from the Block Hei 125, the lowest T_2 signal intensities under three different slug sizes are 80, 102, and 120, respectively. Notably, for Core Sample 23-1 from the Block Hei 71 under a slug size of 0.1 PV, the second peak of the T_2 spectrum curve reaches a maximum signal intensity of 400 and a minimum of 100.

A comparison of the NMR images before and after the water-gas alternating injection in a 1:1 ratio (Figure 6) reveals that regardless of the slug size, the remaining oil content in both core samples decreases significantly. Smaller slug sizes result in less remaining oil and better displacement effect.

Based on the recovery rate calculation results depicted in Figure 7 for the process of 1:1 water-gas alternating slug injection, the following observations can be made: For Core Sample 23-1 from the Block Hei 71, under slug sizes of 0.1 PV, 0.2 PV, and 0.4 PV, the overall final recovery rates reached 75%, 70%, and 70% respectively. The recovery rates for small pores peaked at 31%, 48%, and 40%, with lows of 23%, 39%, and 37% respectively. The recovery rates for large pores peaked at 78%, 60%, and 65%, with lows of 68%, 50%, and 61% respectively. For Core Sample S21 from the Block Hei 125, under slug sizes of 0.1 PV, 0.2 PV, and 0.4 PV, the overall final recovery rates reached 80%, 72%, and 70% respectively. The recovery rates for small pores peaked at 42%, 40%, and 41%, with lows of 35%, 22%, and 22% respectively. The recovery rates for large pores peaked at 68%, 78%, and 78%, with lows of 58%, 58%, and 60% respectively.

These findings highlight the variations in recovery rate across different pore sizes and slug sizes, indicating the complex nature of oil recovery processes and the need for tailored strategies to optimize recovery rates.

Figure 8 shows that the recovery rate gradually decreases as the slug size increases during water-gas alternating slug injection in a 1:1 ratio for the two core samples. Specifically, when the slug size increases from 0.1 PV to 0.4 PV, the average recovery rate decreases by approximately 7%.

3.3 Continuous gas injection at different injection rates

The results of the high-temperature and high-pressure in-line NMR tests for CO_2 flooding in two core samples under continuous gas injection at different injection rates are shown in Figures 9, 10 below.

From Figure 9, it can be observed that during the displacement process of continuous gas injection, except for the T_2 spectrum curves of Core Sample 23-1 from the Block Hei 71 at injection rates of 0.01 mL/min and 0.04 mL/min, which exhibit two peaks, all other conditions show only one prominent peak. The highest peaks of the T_2 signal intensity during the displacement process under all conditions occur at the initial state. For Core Sample 23-1 from the Block Hei 71, the highest peaks of the T_2 signal intensity at

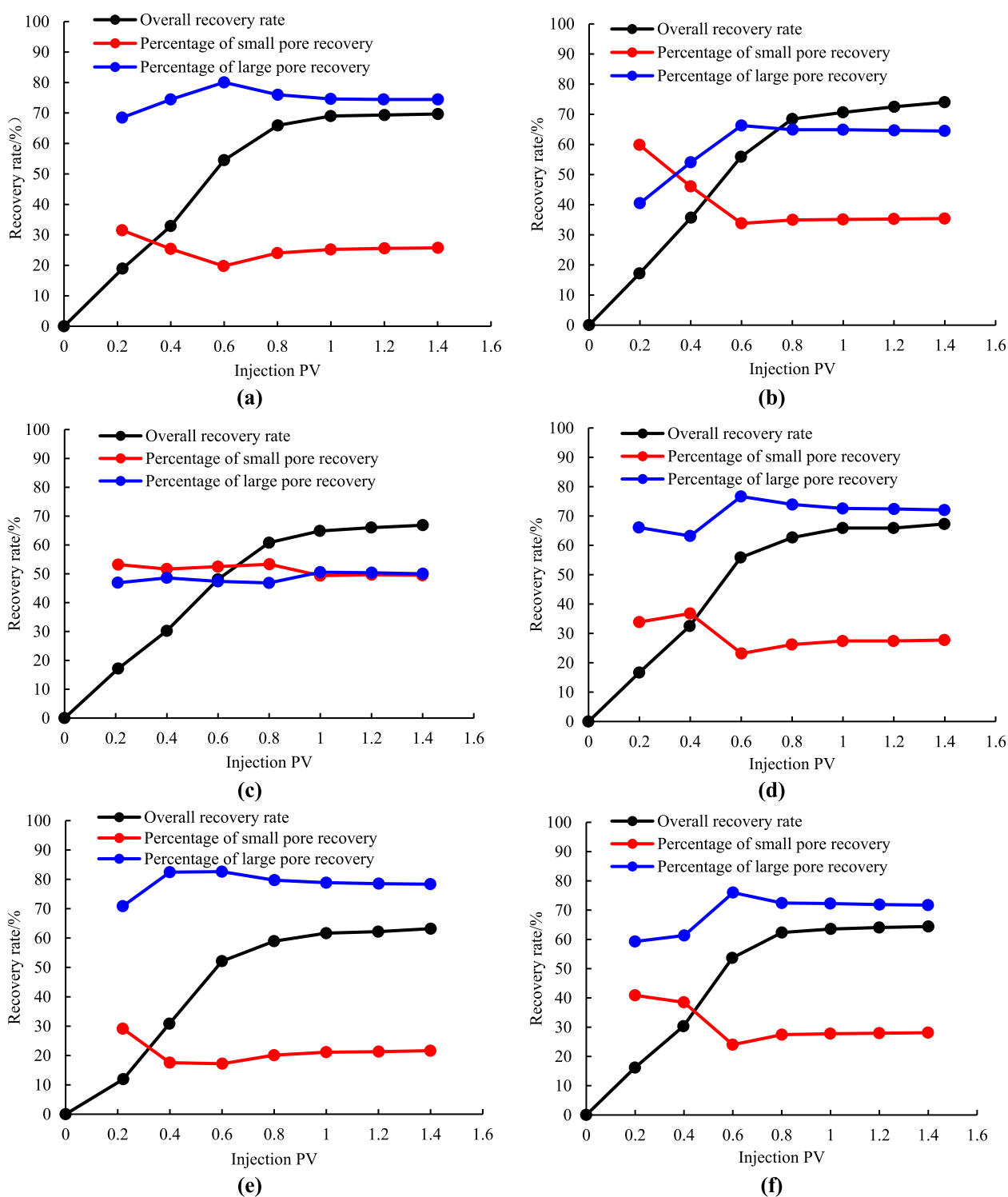
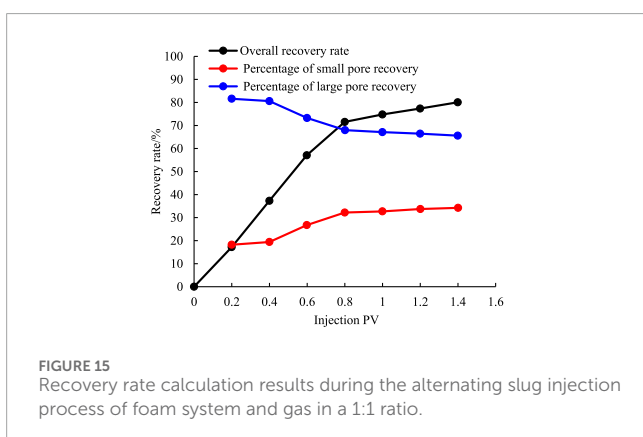
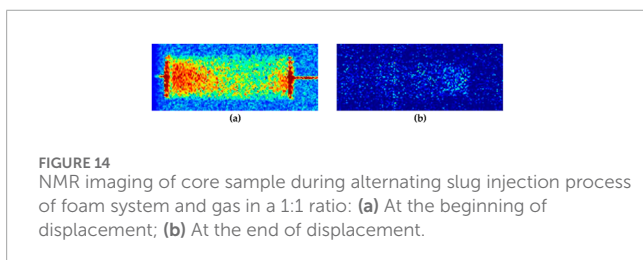
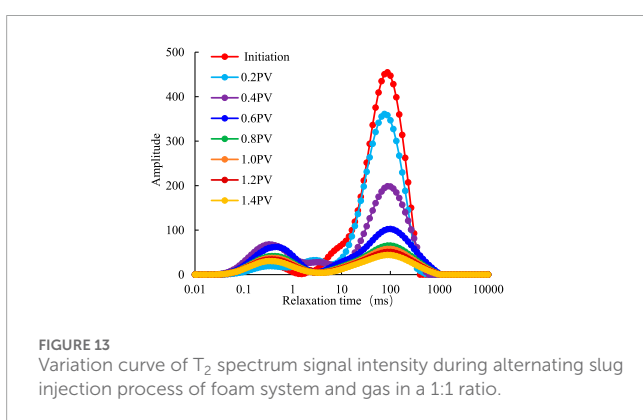
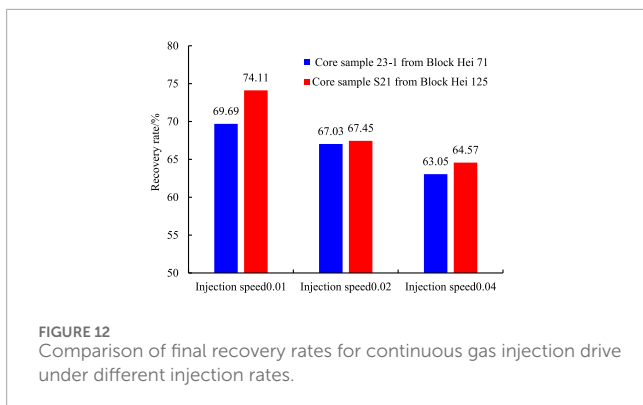


FIGURE 11 Recovery rate calculation results during continuous gas injection at different injection rates: (a) Core sample 23-1 from Block Hei 71, injection rate 0.01 mL/min; (b) Core sample S21 from Block Hei 125, injection rate 0.01 mL/min; (c) Core sample 23-1 from Block Hei 71, injection rate 0.02 mL/min; (d) Core sample S21 from Block Hei 125, injection rate 0.02 mL/min; (e) Core sample 23-1 from Block Hei 71, injection rate 0.04 mL/min; (f) Core sample S21 from Block Hei 125, injection rate 0.04 mL/min.

three different injection rates reach approximately 1,000, 750, and 1,100, respectively. For Core Sample S21 from the Block Hei 125, the highest peaks of the T₂ signal intensity at three different injection

rates all reach around 500. As the displacement time increases, the signal intensity gradually decreases, and the lowest peaks of the T₂ signal intensity occur at the end of the displacement. For Core



Sample 23-1 from the Block Hei 71, the lowest peaks of the T_2 signal intensity at three different injection rates are 300, 280, and 150, respectively. For Core Sample S21 from the Block Hei 125, the lowest peaks of the T_2 signal intensity at three different injection rates are 100, 150, and 125, respectively.

Comparing the NMR images before and after displacement during continuous gas injection at different injection rates (Figure 10), it can be seen that regardless of the injection rate, the remaining oil volume in both core samples decreases significantly. The smaller the injection rate, the less remaining oil there is, indicating a better displacement effect.

From the recovery rate calculations shown in Figure 11 for the continuous gas injection process at different injection rates, we can draw the following conclusions: For Core Sample 23-1 from the Block Hei 71, at injection rates of 0.01 mL/min, 0.02 mL/min, and 0.04 mL/min, the overall final recovery rates are 70%, 68%, and 60%, respectively. The highest recovery rates for small pores reach 31%, 52%, and 30%, while the lowest are 20%, 50%, and 19%. The highest recovery rates for large pores reach 80%, 51%, and 82%, while the lowest are 69%, 49%, and 71%. For Core Sample S21 from the Block Hei 125, at injection rates of 0.01 mL/min, 0.02 mL/min, and 0.04 mL/min, the overall final recovery rates are 73%, 68%, and 65%, respectively. The highest recovery rates for small pores reach 60%, 39%, and 40%, while the lowest are 32%, 21%, and 25%. The highest recovery rates for large pores reach 68%, 78%, and 78%, while the lowest are 40%, 62%, and 60%.

These results indicate that the recovery rates are influenced by both the injection rate and the pore size distribution within the core samples. For Core Sample 23-1 from the Block Hei 71, the overall recovery rate decreases as the injection rate increases, suggesting that a lower injection rate may be more effective in extracting oil from this particular sample. Additionally, the recovery rates for small and large pores vary significantly, indicating that pore size heterogeneity plays a role in oil recovery rate.

Similarly, for Core Sample S21 from the Block Hei 125, the overall recovery rate also decreases as the injection rate increases, although the decrease is less pronounced compared to Core Sample 23-1. The recovery rates for small and large pores also vary, but the trend is less clear, suggesting that factors other than pore size and injection rate may also influence oil recovery in this sample.

From the comparison of the final recovery rates for continuous gas injection drive under different injection rates for the two core samples (Figure 12), it can be observed that the recovery rate gradually decreases as the injection rate increases. When the injection rate is increased from 0.01 mL/min to 0.04 mL/min, the recovery rate decreases by an average of approximately 8%.

3.4 Foam system with gas alternating slug injection in a 1:1 ratio

The foam system with gas alternating slug injection in a 1:1 ratio (with a slug size of 0.1 PV) were specifically applied to Core Sample S21 from the Block Hei 125. The results of the high-temperature and high-pressure online NMR testing for CO_2 flooding on this core sample are shown in Figures 13, 14 below.

From Figure 13, it can be observed that during the alternating slug injection process of the foam system and gas in a 1:1 ratio,

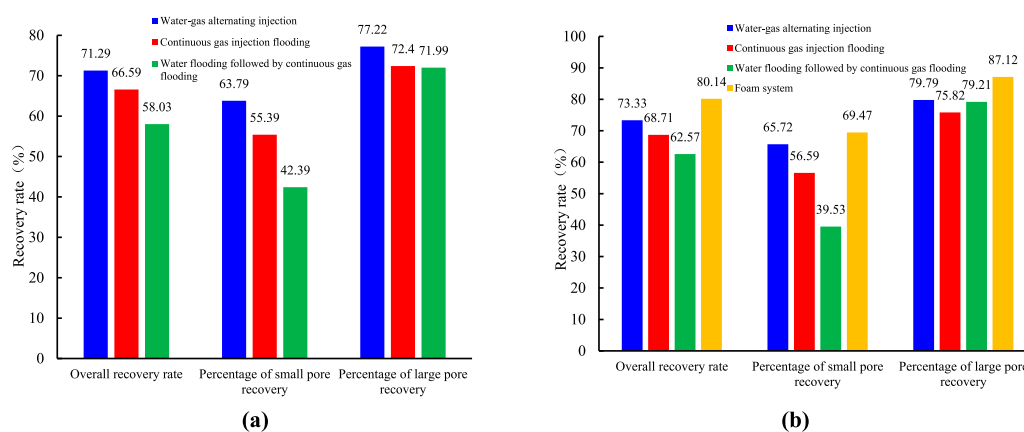


FIGURE 16 Comparison of final recovery rates for different injection methods: (a) Core sample 23-1 from Block Hei 71; (b) Core sample S21 from Block Hei 125.

there are two peaks in the T_2 signal intensity. The highest peak of T_2 signal intensity occurs at the initial state, reaching a value of 450. As the displacement time increases, the T_2 signal intensity gradually decreases. The lowest peak of T_2 signal intensity occurs at 1.4 PV, decreasing to 50.

From the imaging of the displacement process in Figure 14, it can be seen that before the alternating slug injection of the foam system and gas in a 1:1 ratio (with a slug size of 0.1 PV) begins, by observing the core, we can gain a detailed understanding of the initial distribution characteristics of the remaining oil in the core. When the alternating slug injection process ends, imaging of the core reveals that there is still some crude oil remaining in the pores.

From Figure 15, it can be observed that the overall final recovery rates of the alternating slug injection process of the foam system and gas in a 1:1 ratio for rock sample S21 in the Block Hei 125 reaches 80%. The recovery rate for small pores peaks at 35% and reaches a minimum of 19%, while for large pores, it peaks at 82% and reaches a minimum of 68%.

3.5 Comparison of recovery rates between different injection methods

From Figure 16, it can be observed that compared to water flooding followed by continuous gas flooding, the average recovery rate increases by approximately 8% for continuous gas injection, by about 13% for water-gas alternating injection in a 1:1 ratio, and by around 18% for foam system and gas alternating injection in a 1:1 ratio, primarily due to a significant increase in recovery rate for small pores. Overall, the foam system exhibits the highest oil displacement effect, followed by water-gas alternating injection, then continuous gas injection, and finally water flooding followed by continuous gas flooding.

4 Conclusion

(1) The experimental results of water-gas alternating slug injection with different slug sizes indicate that regardless of the slug

size, the remaining oil volume in both rock samples decreases significantly. The smaller the slug size, the less remaining oil there is, and the better the displacement effect. The recovery rate gradually decreases as the slug size increases. When the slug size increases from 0.1 PV to 0.4 PV, the recovery rate decreases by an average of approximately 7%. This can be attributed to the enhanced sweep efficiency achieved with smaller slugs. Smaller slugs allow for more frequent alternating of water and gas phases, which can effectively displace residual oil from the pores of the rock samples. The decrease in remaining oil volume and the corresponding increase in recovery rate with decreasing slug size suggest that optimizing slug size is crucial for enhancing oil recovery using this technique.

- (2) The experimental results of continuous gas injection at different injection rates show that regardless of the injection rate, the remaining oil volume in both rock samples decreases significantly. The lower the injection rate, the less remaining oil there is, and the better the displacement effect. The recovery rate gradually decreases as the injection rate increases. When the injection rate increases from 0.01 mL/min to 0.04 mL/min, the recovery rate decreases by an average of approximately 8%. A slower injection rate allows for more uniform gas distribution within the rock pores, enhancing the gas-oil contact area and facilitating more effective oil displacement. The decrease in recovery rate with increasing injection rate could be due to the creation of gas channels or bypasses that reduce the sweep efficiency of the injected gas.
- (3) The foam system exhibits the highest oil displacement effect, followed by water-gas alternating injection, then continuous gas injection, and finally water flooding followed by continuous gas flooding. Compared to water flooding followed by continuous gas flooding, the average recovery rate increases by approximately 8% for continuous gas injection, by about 13% for water-gas alternating slug injection, and by around 18% for the foam system. The comparison among different EOR techniques highlights the superiority of the foam system

in terms of oil recovery. The foam system's ability to generate stable foams that can effectively block high-permeability zones and redirect the injected gas towards the oil-bearing regions contributes to its high oil displacement effect.

While the NMR tests provided valuable insights into fluid dynamics during CO₂ flooding, several limitations should be noted. The core samples used in this study may not fully represent the heterogeneity of the Daqingzijing Oilfield, and the NMR measurements were conducted under simplified conditions that did not account for all *in situ* factors. Future work could benefit from more extensive sampling and the inclusion of additional geophysical techniques for a more comprehensive understanding of the CO₂ flooding process.

This study demonstrates the feasibility of using high-temperature and high-pressure online NMR testing to monitor CO₂ flooding in the Daqingzijing Oilfield. The results highlight the potential of NMR to provide real-time data on fluid saturation changes, which can inform optimization strategies for EOR projects. Future research should focus on refining NMR methods and integrating them with other monitoring techniques to enhance the overall understanding and efficiency of CO₂-based EOR.

Data availability statement

The raw data supporting the conclusions of this article will be made available by the authors, without undue reservation.

Author contributions

YW: Writing–original draft, Writing–review and editing. ZB: Writing–original draft, Writing–review and editing. ZL: Writing–review and editing. SH: Writing–review and editing. FF: Writing–review and editing.

References

- Chen, H., Wang, B., Li, T., Zhang, X., Zhu, J., Dai, Z., et al. (2024). Optimization of fractured shale oil energized imbibition huff and puff process by on-line nuclear magnetic resonance monitoring method. *Oil Drill. and Prod. Technol.* 46 (02), 228–237. doi:10.13639/j.odpt.202405025
- Ding, S., Zhang, M., Li, Y., Xu, C., Zhou, Y., Gao, Q., et al. (2024). Sensitivity analysis of injection-production parameters for CO₂ huff-n-puff flooding and storage in tight oil reservoirs: a case from typical tight reservoirs of Chang 7 Member, Ordos Basin. *Xinjiang Pet. Geol.* 45 (02), 181–188. doi:10.7657/XJPG20240206
- Dong, W. (2023). *Study on reservoir heterogeneity of the 1st member of qingshankou formation in daqingzijing oilfields in jilin province*. Beijing: China University of Petroleum. doi:10.27643/d.cnki.gsybu.2023.000936
- Dong, Y., Wang, R., Wang, S., Meng, W., Chen, L., and Tang, S. (2022). Study on synergistic oil displacement mechanism of CO₂-low interfacial tension viscoelastic fluid alternating flooding in ultra-low permeability sandstone reservoir. *Chem. Eng. Oil and Gas* 51 (06), 77–83. doi:10.3969/j.issn.1007-3426.2022.06.011
- Duan, X., Hu, Z., Gu, Z., Chang, J., Shen, R., Sun, W., et al. (2021). Study on the production laws of shale gas in different occurrence states in the use of NMR online detection technology. *Nat. Gas. Ind.* 41 (05), 76–83. doi:10.3787/j.issn.1000-0976.2021.05.008
- Fu, L. (2023). NMR online experiment for dynamic imbibition drainage of tight sandstone: a case study of Fuyu reservoir in northern Songliao Basin. *Petroleum Geol. and Oilfield Dev. Daqing* 42 (03), 66–74. doi:10.19597/j.ISSN.1000-3754.202204011
- Gao, H. (2019). Reservoir evaluation of Hei 124 block in Daqingzijing oilfield. *Pet. Knowl.* (05), 58–59.
- Guo, H., Du, M., Yao, J., Wang, Z., Zhang, J., and Liu, H. (2024). Numerical simulation study on optimization of CO₂ flooding parameters in Yanchang low permeability reservoir. *Unconv. Oil and Gas* 11 (01), 78–84. doi:10.19901/j.fcgyq.2024.01.10
- Hu, R., Wan, J., Kim, Y., and Tokunaga, T. (2017). Wettability effects on supercritical CO₂-brine immiscible displacement during drainage: pore-scale observation and 3D simulation. *Int. J. Greenh. Gas Control* 60, 129–139. doi:10.1016/j.ijggc.2017.03.011
- Kamali, F., Hussain, F., and Cinar, Y. (2015). A laboratory and numerical-simulation study of co-optimizing CO₂ storage and CO₂ enhanced oil recovery. *SPE J.* 20, 1227–1237. doi:10.2118/171520-PA
- Lan, J., Tang, F., Xie, D., Liang, X., Mao, J., and Wang, G. (2023). Study on enhanced oil recovery by CO₂ flooding in tight oil reservoirs. *Contemp. Chem. Ind.* 52 (04), 997–1001. doi:10.13840/j.cnki.cn21-1457/tq.2023.04.006
- Liang, M., Yuan, H., Yang, Y., Lin, J., and Yang, Y. (2016). Review on the mechanisms during CO₂ flooding process. *Petrochem. Ind. Appl.* 35 (06), 1–5+9. doi:10.3969/j.issn.1673-5285.2016.06.001
- Liu, Y., Teng, Y., Jiang, L., Zhao, J., Zhang, Y., Wang, D., et al. (2017). Displacement front behavior of near miscible CO₂ flooding in decane saturated synthetic sandstone cores revealed by magnetic resonance imaging. *Magn. Reson. Imaging* 37, 171–178. doi:10.1016/j.mri.2016.12.003

Funding

The author(s) declare that financial support was received for the research and/or publication of this article. This research was funded by the General Program of National Natural Science Foundation of China (52274034); the General Program of Chongqing Natural Science Foundation (CSTB2022NSCQ-MSX1423); the Chongqing Municipal Education Commission Science and Technology Research Plan Project (KJQN202301537).

Conflict of interest

Author YW was employed by Research Institute of Petroleum Exploration and Development, PetroChina. Authors ZB and ZL were employed by Research Institute of Exploration and Development, PetroChina Jilin Oilfield Company.

The remaining authors declare that the research was conducted in the absence of any commercial or financial relationships that could be construed as a potential conflict of interest.

Generative AI statement

The author(s) declare that no Generative AI was used in the creation of this manuscript.

Publisher's note

All claims expressed in this article are solely those of the authors and do not necessarily represent those of their affiliated organizations, or those of the publisher, the editors and the reviewers. Any product that may be evaluated in this article, or claim that may be made by its manufacturer, is not guaranteed or endorsed by the publisher.

- Liu, Z., Zhang, W., Sun, J., Zhang, P., and Chang, X. (2018). Factors influencing the physical properties of reservoir in the Qing 1 section of Daqingzijing Oilfield. *J. Xi'an Univ. Sci. Technol.* 38 (01), 99–107. doi:10.13800/j.cnki.xakjdxsb.2018.0115
- Lu, M., Qian, Q., Zhong, A., Zhang, Z., and Zhang, L. (2024). Investigation on the flow behavior and mechanisms of water flooding and CO₂ immiscible/miscible flooding in shale oil reservoirs. *J. CO₂ Util.* 80, 102660. doi:10.1016/j.jcou.2023.102660
- Tang, F., Zhu, Y., Zhang, Y., Meng, W., Zhang, T., and Xu, C. (2021). Experimental research of the effect of CO₂ injection on porous media and fluid property in reservoir. *Chem. Eng. Oil and Gas* 50 (1), 72–76+82. doi:10.3969/j.issn.1007-3426.2021.01.012
- Tang, H., Zhang, W., Peng, D., Lu, H., Tang, H., and Zhou, Y. (2022). Experimental study on the reaction of kaolinite with CO₂ (aq). *Chem. Eng. Oil and Gas* 51 (05), 104–109. doi:10.3969/j.issn.1007-3426.2022.05.016
- Torabi, F., Jamaloei, B., Zarivnyy, O., Paquin, B., and Rumpel, N. (2012). The evaluation of variable-injection rate waterflooding, immiscible CO₂ flooding, and water-alternating-CO₂ injection for heavy oil recovery. *Liq. Fuels Technol.* 30 (16), 1656–1669. doi:10.1080/10916466.2010.509067
- Wang, C., Tang, Q., Li, S., and Zhao, S. (2017). Application of new generation NMR analyzer in rapid evaluation of raw oil. *Petroleum Process. Petrochem.* 48 (10), 101–106.
- Xu, H., Zhang, X., Liu, R., Xia, J., Wang, Q., and Dong, H. (2024). CO₂ immiscible flooding technology for medium-deep heavy oil of Bei 10 well block in eastern Junggar Basin. *Petroleum Geol. and Oilfield Dev. Daqing* 43 (01), 142–148. doi:10.19597/J.ISSN.1000-3754.20230800